Environmental Science & Technology

pubs.acs.org/est

Article

Fate and Transport of Mercury through Waterflows in a Tropical Rainforest

Wei Yuan, Xun Wang,* Che-Jen Lin, Ge Zhang, Fei Wu, Nantao Liu, Longyu Jia, Hui Zhang, Huazheng Lu, Jinlong Dong, and Xinbin Feng*

Cite This: *Environ. Sci. Technol.* 2024, 58, 4968−4978

Read Online

ACCESS | Metrics & More | Article Recommendations | SI Supporting Information

ABSTRACT: Knowledge gaps of mercury (Hg) biogeochemical processes in the tropical rainforest limit our understanding of the global Hg mass budget. In this study, we applied Hg stable isotope tracing techniques to quantitatively understand the Hg fate and transport during the waterflows in a tropical rainforest including open-field precipitation, throughfall, and runoff. Hg concentrations in throughfall are 1.5−2 times of the levels in open-field rainfall. However, Hg deposition contributed by throughfall and open-field rainfall is comparable due to the water interception by vegetative biomasses. Runoff from the forest shows nearly one order of magnitude lower Hg concentration than those in throughfall. In contrast to the positive Δ^{199}Hg and Δ^{200}Hg signatures in open-field rainfall, throughfall water exhibits nearly zero signals of Δ^{199}Hg and Δ^{200}Hg, while runoff shows negative Δ^{199}Hg and Δ^{200}Hg signals. Using a binary mixing model, Hg in throughfall and runoff is primarily derived from atmospheric Hg^0 inputs, with average contributions of 65 ± 18 and 91 ± 6%, respectively. The combination of flux and isotopic modeling suggests that two-thirds of atmospheric Hg^{2+} input is intercepted by vegetative biomass, with the remaining atmospheric Hg^{2+} input captured by the forest floor. Overall, these findings shed light on simulation of Hg cycle in tropical forests.

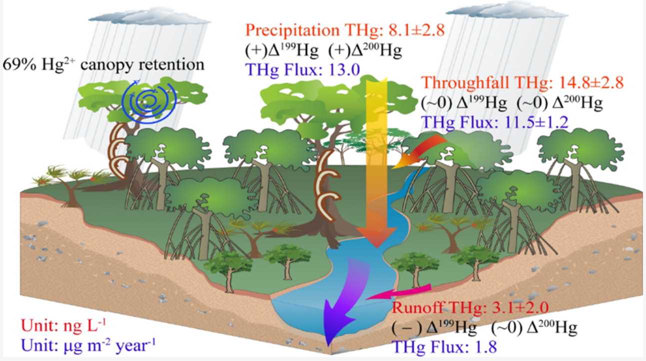

KEYWORDS: *mercury isotope, wet deposition, throughfall, runoff, tropical rainforest*

1. INTRODUCTION

Mercury (Hg) is a global pollutant. There are mainly two forms of Hg in the atmosphere, namely, gaseous elemental mercury (Hg^0) and oxidized Hg (Hg^{2+}). Hg^{2+} is active and can be quickly scavenged from air via wet or dry deposition in several days to weeks.[1,2] Hg^0 accounts for more than 95% of total Hg in the air and has a 0.5−1.5 year atmospheric residence time due to its high vapor pressure and low oxidation potential.[2,3] Atmospheric Hg^0 can be assimilated by vegetation and then deposition into soil via litterfall[4−6] and also oxidized to Hg^{2+} and then deposition into remote ecosystems.[7,8] The increasing atmospheric Hg deposition in remote ecosystems poses an increasing concern of Hg pollution across the globe.[9−11]

Forests act as an important Hg sink due to up to global 2200−3400 Mg $year^{-1}$ atmospheric total Hg deposition.[12] Tropical rainforests account for 45% of the global forest areas.[13] Yet, observations and understanding of Hg cycling in this terrestrial ecosystem remain limited.[12,14−17] Given the climate and canopy structure in contrast to other forest types, Hg biogeochemical cycles in tropical rainforests may exhibit unique features. Tropical rainforests have a canopy height up to 60−70 m, a large amount of biomass, and usually >2000 mm open-field rainfall amount.[18,19] The canopy structure and high precipitation may increase atmospheric Hg deposition.

The water cycle, including rainfall and throughfall (rainfall passing through the forest canopy) and runoff, can shape Hg^{2+} deposition and output flux of Hg^{2+} in forests.[20−22] The ratio of throughfall Hg concentration over open-field rainfall Hg concentration in Amazon remote tropical rainforests is in the range of 2−4[23,24] while 1−2 for most subtropical, temperate, and boreal forests.[12,25,26] However, the runoff in the tropical rainforest is typically deficient in Hg concentration (<5 ng L^{-1}) and distinctly low in Hg flux (<5 μg m^{-2} $year^{-1}$).[23,27] Such unique characteristics of Hg input and output warrant investigation on Hg transport via waterflow in tropical rainforests.

Additionally, there were distinct knowledge gaps on the fate of atmospheric Hg^0 and Hg^{2+} in forests. Previously deposited

Received: November 6, 2023
Revised: February 26, 2024
Accepted: February 27, 2024
Published: March 7, 2024

https://doi.org/10.1021/acs.est.3c09265
Environ. Sci. Technol. 2024, 58, 4968−4978

Hg on the surface of foliage can be washed off into throughfall in the process of water passing through the canopy.[28−30] Thus, throughfall Hg deposition was usually regarded as a proxy for atmospheric Hg^{2+} deposition in forest ecosystems.[12,26,31,32] However, the recent studies suggest that throughfall Hg deposition is not a good proxy for atmospheric Hg^{2+} deposition because Hg^0 uptake by the canopy and the subsequent detritus mixing into precipitation contribute a large fraction of throughfall Hg deposition.[33−35] Additionally, Hg in the runoff of temperate and boreal forests likely originates from the atmospheric Hg^0 deposition stored in degraded vegetative biomass where Hg is bound by organic soil rather than from atmospheric Hg^{2+} deposition.[36,37] There are still large uncertainties due to the absence of continuous monitoring in the whole hydrological year or lack of observations at the ecosystem scale. Hence, the source of Hg in throughfall and runoff in forest ecosystems, specifically in tropical rainforests, remains unknown.

Signatures of stable Hg isotopes, reported as the mass-dependent fractionation (MDF, reported as δ^{202}Hg) and mass-independent fractionation (MIF, reported as Δ^{199}Hg and Δ^{201}Hg for odd-MIF and Δ^{200}Hg and Δ^{204}Hg for even-MIF), are an effective signal to trace the Hg sources and biogeochemical processes in throughfall and runoff.[36,38] Precipitation Hg usually displays negative δ^{202}Hg and unique positive Δ^{199}Hg (~0.50‰ of mean value) and Δ^{200}Hg signals (~0.25‰ of mean value).[39−42] Hg in forest foliage and surface soil usually has negative δ^{202}Hg, distinct negative Δ^{199}Hg (−0.50 to −0.20‰), and slightly negative Δ^{200}Hg signatures (−0.08 to −0.02‰).[12,35,43−47] The hydrological processes in throughfall and runoff do not produce even-MIF.[48,49] Therefore, we can use the Δ^{200}Hg signatures to construct the Hg source tracing model to improve our knowledge of Hg fate in throughfall and runoff.

This study aims to quantify the source contributions and fate of Hg in throughfall and runoff to better quantify the deposition of atmospheric Hg^{II} using data of Hg flux and isotopic signatures in a Chinese tropical rainforest. We measured the concentration and the associated isotopic signatures of different Hg species (THg, DHg, and PHg) and calculated the cumulative Hg flux over a hydrological year. The cycle and implication of atmospheric Hg^0 deposition and precipitation Hg^{II} retention occurring on the canopy in a tropical rainforest are discussed.

2. MATERIALS AND METHODS

2.1. Site Description. Our study site locates at the Bu-Beng Tropical Forest Dynamic station (BB, 21° 36′ 42.05″N, 101° 34′ 57.72″E, and 711−737 m above the sea level) of Mengla, Xishuangbanna, Yunnan Province in Southwest China. BB has a tropical monsoon climate with an annual mean temperature of 22.5 °C and precipitation of 1650 mm.[50] Up to 80% of the total annual precipitation occurs during the rainy season (May to October). The year-round frost-free condition is a representative feature of a tropical climate. The forest at BB has a typical canopy structure of rainforest including the canopy layer, understory layer, and undergrowth layer. The dominant tree species in the canopy layer are *Parashorea chinensis* and *Pometia tomentosa*, which are representative tropical plants with a canopy height of 60−65 m and account for >45% of total foliage biomass.[19,51] The dominant tree species in the understory layer are *Pittosporopsis kerrii*, *Baccaurea ramiflora*, and *Cleidion brevipetiolatum*, and the dominant tree species in the undergrowth layer are *Saprosma ternate* and *Alpinia conchigera*.[50,52] A small valley passes through our studied site, and the south side of the valley has relatively more intensive canopy height compared to the north side of the valley (details in Figure S1). The whole catchment area is 373,645 m^2.

2.2. Sample Collections. The open-field rainfall samples were collected just outside of the forest. Two sites were prepared for collecting throughfall samples at the south and north sides of the valley, respectively. The open-field precipitation, throughfall, and runoff samples were collected every 10 days from August 2021 to July 2022 to explore the monthly variations. Additionally, we sampled each event of precipitation, throughfall, and runoff samples in August 2021 (i.e., rainy season), November to December 2021, and March 2022 (i.e., dry season) for measurements of Hg isotopic signatures. We recorded the quantities of rainfall and throughfall continuously by tipping bucket rain gauges automatically (Onset, HOBO RG3-M).

The protocols for sample collections have been described in our earlier work.[9,33,53] Briefly, we used 0.4 g of chlorine-impregnated activated carbon (ClC) traps with a flow rate of 1.5 L min^{-1} to collect the Hg^0 of air gas every 10 days from August 2021 to July 2022. Additionally, we collected the precipitation, throughfall (south and north), and runoff samples by using a 1.35 m^2 stainless steel rain board covered by the 0.3 mm Teflon film. A 5 L borosilicate glass bottle was cleaned with 60% aqua regia and distilled water successively before each field collection. After collection, 50 mL of water sample was transferred into a Hg-free fluorinated ethylene propylene (FEP) bottle for total Hg analysis. Another 50 mL of water sample was filtered with a 0.45 μm polyethersulfone filter membrane and then transferred into a Hg-free FEP bottle for dissolved Hg (DHg) analysis. All samples were preserved with 0.25 mL of ultraclean grade HCl, double-packed in Ziploc bags and stored in a refrigerated chamber, and transported back to the laboratory for further analysis of Hg and dissolved organic carbon (DOC).

Given the 5−10 ng Hg mass needed for measuring Hg isotopic compositions, we collected 10 L rainfall, throughfall, and runoff samples to ensure sufficient Hg mass in each sample. The preconcentration of DHg and particulate Hg (PHg) from the water sample follows the protocol developed in our previous study.[53] Briefly, the water samples were filtered by microglass filters (Munktell, Sweden) to collect PHg, and DHg was preconcentrated by adding BrCl and $SnCl_2$ to reduce Hg^{2+} into Hg^0 vapor and punching into 0.4 g of chlorine-impregnated activated carbon (ClC) trap. The microglass filter was placed in a 450 °C-muffle furnace for 2 h to remove any potentially absorbed Hg before field experiments.

2.3. Measurements of Hg Concentration and Isotope. The concentration of total Hg and dissolved Hg in each water sample was determined by following US EPA Method 1631.[9,33,54] The Hg concentration analytic uncertainty was 1.0 ng L^{-1}. Hg in the blank solution of rain board and bottle blank solution was below 0.01 ng L^{-1} ($n = 12$), which was less than 2% of total Hg concentrations in water samples. In addition, the average concentration of Hg for the reagent blank and measurement system blank was 0.02 ± 0.02 ng L^{-1} ($n = 6$). The DOC concentration in water was determined using a total organic carbon analyzer (Shimadzu, Japan, detection limit of 4 μg L^{-1}).

https://doi.org/10.1021/acs.est.3c09265
Environ. Sci. Technol. 2024, 58, 4968−4978

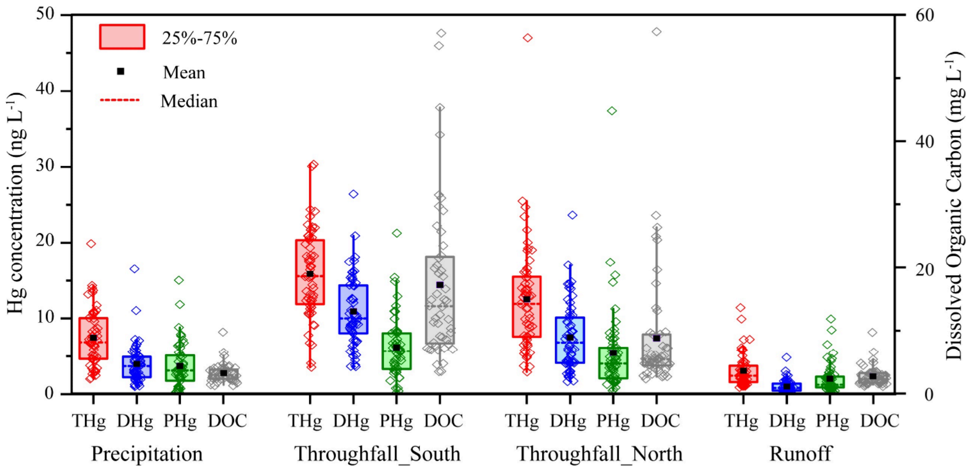

Figure 1. Total mercury (THg), dissolved mercury (DHg), particulate mercury (PHg), and dissolved organic carbon (DOC) in precipitation, throughfall (south and north sides of the watershed), and runoff.

The measurement of Hg isotopic compositions in samples collected in ClC traps and on microglass filter (representing particulate Hg) had been described in our earlier studies.[9,33,53] All samples were processed by double-stage heating pyrolysis in a tube muffle furnace for Hg preconcentration.[55,56] The preconcentrated Hg solution (40% reverse aqua regia, HNO_3/HCl = 2:1, v/v) was diluted to 0.5 ng mL^{-1} prior to Hg isotope measurements. The recoveries of preconcentration were in the range of 88−96% (92.2 ± 2.9%, $n = 6$) for the standard vegetative reference material (Lichen, BCR-482 with a Hg content of 480 ± 20 ng g^{-1}) and 92−105% (97.8 ± 4.9%, $n = 6$) for the soil reference material (GSS-4 with a Hg content of 590 ± 30 ng g^{-1}). The recovery of Hg in trapping solution was 95.5 ± 8.9% (range of 85−115%, $n = 71$, detailed in Tables S1−S3). Additionally, the blank of ClC traps was 150−300 pg g^{-1}, less than 5% of the amount loaded after experiments.

Hg isotopic compositions were measured by a multicollector inductively coupled plasma mass spectrometer (MC-ICPMS, Nu II, Nu Instruments, UK). Concentrations and acid matrices of Hg standard solutions (NIST-3133 and NIST-8610 as the secondary standard solution) were also matched to those of the sample solutions. Following the calculation of Bergquist and Blum,[57] δ^{202}Hg is reported as

$$\delta^{202}\mathrm{Hg}(‰) = [(^{202}\mathrm{Hg}/^{198}\mathrm{Hg})_{\mathrm{sample}}/(^{202}\mathrm{Hg}/^{198}\mathrm{Hg})_{\mathrm{ref}} - 1] \times 1000 \quad (1)$$

MIF is calculated as

$$\Delta^{xx}_{x}\mathrm{Hg}(‰)=\delta^{xx}_{x}\mathrm{Hg} - \delta^{202}\mathrm{Hg} \times \beta_{xxx} \quad (2)$$

where β_{xxx} values are 0.2520 for ^{199}Hg, 0.5024 for ^{200}Hg, 0.7520 for ^{201}Hg, and 1.4930 for ^{204}Hg. The isotopic signatures of the NIST-8610 standard, which were measured every 10 samples, were determined to be δ^{202}Hg = −0.5 ± 0.08‰, Δ^{199}Hg = −0.02 ± 0.09‰, Δ^{200}Hg = 0.02 ± 0.08‰, Δ^{201}Hg = −0.04 ± 0.08‰, and Δ^{204}Hg = 0.03 ± 0.16‰ (mean ± 2σ, $n = 20$). The measured isotope signatures of the BCR-482 standard were δ^{202}Hg = −1.58 ± 0.12‰, Δ^{199}Hg = −0.63 ± 0.13‰, Δ^{200}Hg = 0.05 ± 0.05‰, Δ^{201}Hg = −0.63 ± 0.12‰, and Δ^{204}Hg = −0.16 ± 0.10‰ ($n = 5$), and those of the GSS-4 standard were δ^{202}Hg = −1.74 ± 0.12‰, Δ^{199}Hg = −0.42 ± 0.09‰, Δ^{200}Hg = −0.04 ± 0.10‰, and Δ^{201}Hg = 0.12 ± 0.11‰ ($n = 5$). All Hg isotopic signatures of these certificated reference materials were consistent with the reported values.[9,58] The analytic uncertainty of BCR-482 was applied to represent the sample isotopic uncertainties due to the largest uncertainty of replicate analyses of BCR-482.

2.4. Hg Isotopic Mixing Model.

We suggested geogenic Hg as the negligible source in runoff. There are two reasons to support this hypothesis. One is that geogenic Hg is mainly fixed in the soil minerals and hardly dissolves into water.[59] The other is that much more negative signatures of δ^{202}Hg and Δ^{199}Hg in runoff water than the isotopic features in bedrock (δ^{202}Hg = −0.42 ± 0.19‰ and Δ^{199}Hg = −0.09 ± 0.03‰)[50] also confirm negligible contribution from geogenic Hg. Hg in throughfall and surface runoff comes primarily from atmospheric Hg^0 and Hg^{2+}. The hydrological process of throughfall and runoff does not cause even-MIF.[48,49] Therefore, the Δ^{200}Hg signal is conserved and can be used for estimating the source contributions to throughfall and runoff samples as follows:

$$F_{\mathrm{Hg}^0} + F_{\mathrm{Hg}^{2+}} = 1 \quad (3)$$

$$F_{\mathrm{Hg}^0} \times \Delta^{200}\mathrm{Hg}^0 + F_{\mathrm{Hg}^{2+}} \times \Delta^{200}\mathrm{Hg}^{2+} = \Delta^{200}\mathrm{Hg}_{\mathrm{sample}} \quad (4)$$

where F_{Hg^0} is the fraction of atmospheric Hg^0 input, and $F_{\mathrm{Hg}^{2+}}$ is the fraction of atmospheric Hg^{2+} input. $\Delta^{200}\mathrm{Hg}^0$ is the isotopic signature of atmospheric Hg^0 inputs. $\Delta^{200}\mathrm{Hg}^{2+}$ is the isotopic signature of atmospheric Hg^{2+} inputs. $\Delta^{200}\mathrm{Hg}_{\mathrm{sample}}$ represents the isotopic signatures of throughfall and runoff. We used the Δ^{200}Hg signal of DHg in precipitation as the endmember of DHg in throughfall and runoff and the Δ^{200}Hg signal of PHg in precipitation as the endmember of PHg in throughfall and runoff. Two methods were applied to calculate the source contributions. One is to average the isotopic values of each sample before calculation (eqs 3 and 4). The other is to calculate the contribution of each sample (in Tables S2 and S3) and then average them. Two methods showed the consistent results in Table S5, and the method 2 result was applied in this study. To quantify the mean results and uncertainties of the model, Monte Carlo simulation was applied in 100,000 simulations with normal distribution (around 1σ) random variation of Hg isotopic signatures using Rstudio (Section S1). The model uncertainties are discussed in detail in Section S2 of the Supporting Information.

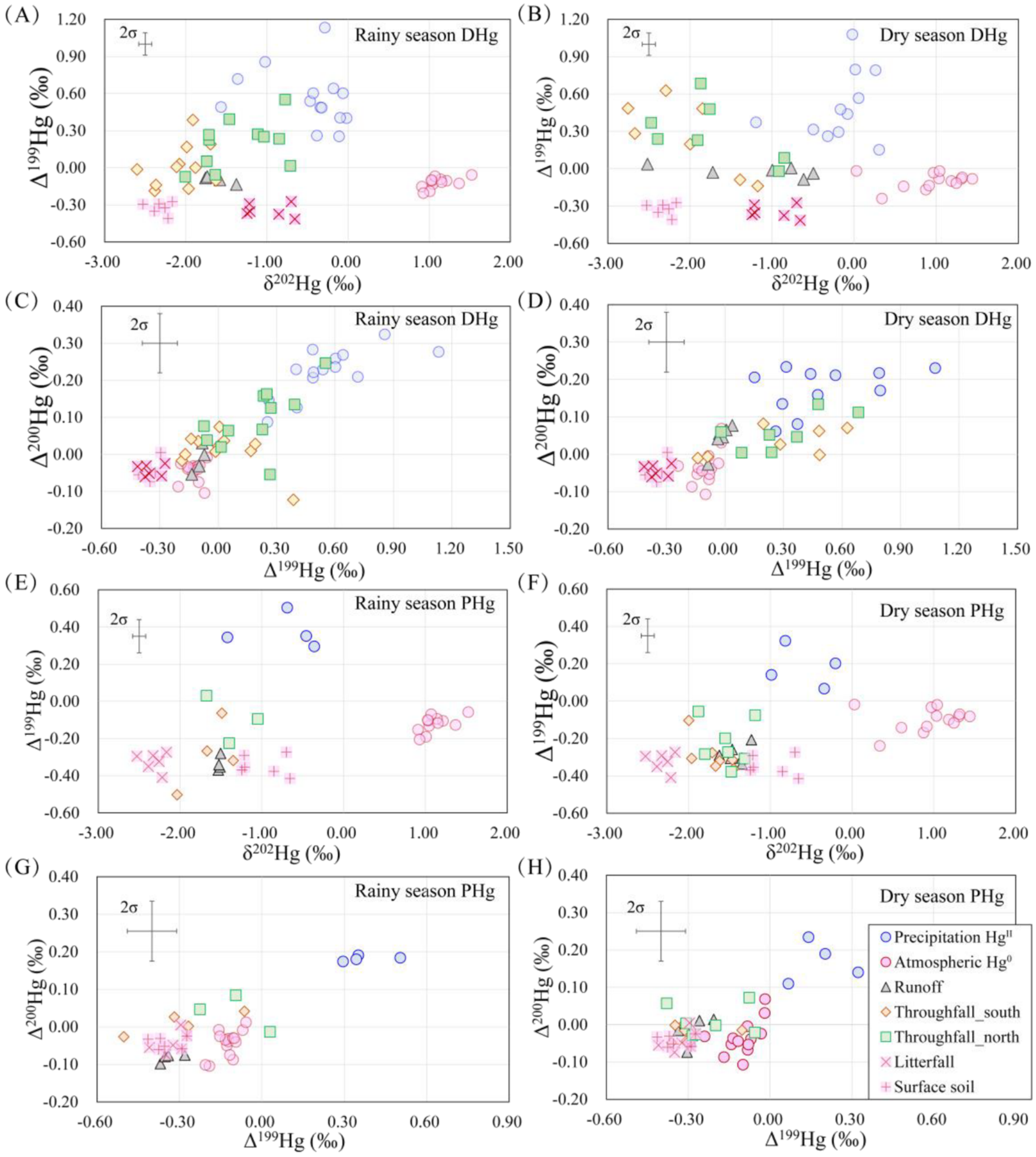

Figure 2. Hg isotopic compositions in litterfall, surface soil, atmospheric Hg^0, precipitation Hg^{II}, throughfall, and runoff. (A) $\Delta^{199}Hg$ versus $\delta^{202}Hg$ for DHg in the rainy season, (B) $\Delta^{199}Hg$ versus $\delta^{202}Hg$ for DHg in the dry season, (C) $\Delta^{200}Hg$ versus $\Delta^{199}Hg$ for DHg in the rainy season, (D) $\Delta^{200}Hg$ versus $\Delta^{199}Hg$ for DHg in the dry season, (E) $\Delta^{199}Hg$ versus $\delta^{202}Hg$ for PHg in the rainy season, (F) $\Delta^{199}Hg$ versus $\delta^{202}Hg$ for PHg in the dry season, (G) $\Delta^{200}Hg$ versus $\Delta^{199}Hg$ for PHg in the rainy season, and (H) $\Delta^{200}Hg$ versus $\Delta^{199}Hg$ for PHg in the dry season. The litterfall and surface soil isotopic data were from Xia et al.[50] The error bars represent ±2 standard deviation.

2.5. Hg Flux Budget in Water. Combining the Hg isotopic model results and Hg concentrations and fluxes, the atmospheric Hg^0 and Hg^{2+} mass flows were estimated as follows:

$$\mathrm{TFlux}_{Hg^0} = \sum (\mathrm{Flux}_{DHg} \times F_{Hg^0\_DHg} + \mathrm{Flux}_{PHg} \times F_{Hg^0\_PHg}) \qquad (5)$$

$$\mathrm{TFlux}_{Hg^{2+}} = \sum (\mathrm{Flux}_{DHg} \times F_{Hg^{2+}\_DHg} + \mathrm{Flux}_{PHg} \times F_{Hg^{2+}\_PHg}) \qquad (6)$$

where TFlux_{Hg^0} and $\mathrm{TFlux}_{Hg^{2+}}$ represent the annual total Hg^0 and Hg^{2+} flux in throughfall and runoff, respectively. Flux_{DHg} and Flux_{PHg} represent the DHg and PHg flux, respectively. $F_{Hg^0\_DHg}$ and $F_{Hg^{2+}\_DHg}$ represent the fraction of atmospheric Hg^0 and Hg^{2+} in DHg, respectively. $F_{Hg^0\_PHg}$ and $F_{Hg^{2+}\_PHg}$ represent the fraction of atmospheric Hg^0 and Hg^{2+} in PHg, respectively. Then, we estimated the lower limit of atmospheric Hg^{2+} canopy retention flux (i.e., CRFlux) and forest floor retention flux (i.e., FRFlux) as

$$\mathrm{CRFlux}_{Hg^{2+}} = \mathrm{Flux}_{Hg^{2+}\_pre} - \mathrm{TFlux}_{Hg^{2+}\_thr} \qquad (7)$$

$$\mathrm{FRFlux}_{Hg^{2+}} = \mathrm{Flux}_{Hg^{2+}\_thr} - \mathrm{TFlux}_{Hg^{2+}\_run} \qquad (8)$$

where $\mathrm{Flux}_{Hg^{2+}\_pre}$ represents the annual open-field precipitation deposition flux. $\mathrm{TFlux}_{Hg^{2+}\_thr}$ refers to the throughfall Hg^{2+} deposition, and $\mathrm{TFlux}_{Hg^{2+}\_run}$ is the total atmospheric

https://doi.org/10.1021/acs.est.3c09265
Environ. Sci. Technol. 2024, 58, 4968−4978

Hg^{2+}-contributed flux in runoff. More details about the assumption of eqs 7 and 8 can be found in Section 4.3.

3. RESULTS

3.1. Distribution of Hg Concentration for Each Species. The mean THg in open-field precipitation was 8.1 ± 2.8 ng L^{-1}, including 4.0 ± 1.9 ng L^{-1} of DHg and 4.1 ± 2.2 ng L^{-1} of PHg (Figure 1). The mean DHg concentration in the rainy season was significantly lower than the concentration in the dry season (3.5 ± 1.7 ng L^{-1} versus 4.7 ± 1.9 ng L^{-1}; $p < 0.05$, independent-samples *t* test). However, PHg concentrations were comparable (4.3 ± 2.1 ng L^{-1} versus 3.9 ± 2.5 ng L^{-1}).

The THg concentrations in throughfall were 16.2 ± 5.2 ng L^{-1} for the south side and 13.5 ± 5.0 ng L^{-1} for the north side of the watershed, 1.5−2 times the Hg concentration in corresponding open-field precipitation. The DHg concentration in throughfall at the south side was significantly higher than the DHg concentration of the north side (9.8 ± 4.2 ng L^{-1} vs 7.4 ± 3.3 ng L^{-1}, $p < 0.01$, independent-samples *t* test), while the PHg concentrations were comparable (6.4 ± 3.5 ng L^{-1} versus 6.2 ± 3.8 ng L^{-1}, $p > 0.05$, independent-samples *t* test).

The throughfall THg and DHg concentrations in the dry season (16.3 ± 5.0 and 9.7 ± 4.8 ng L^{-1}) were significantly higher than values in the rainy season (13.7 ± 4.5 and 7.7 ± 3.1 ng L^{-1}; $p < 0.05$, independent-samples test). The seasonal trend of throughfall PHg concentration is not significant. The mean THg concentration in runoff was 3.1 ± 2.1 ng L^{-1} and showed no seasonal trend. The ratios of DHg/PHg were 1:2 in runoff, 1:1 in precipitation, and 1.2−1.5:1 in throughfall.

3.2. Variations of Hg Flux of Each Species. With the annual 1576 mm precipitation in the hydrological year (Figure S2), the open-field rainfall Hg deposition flux was estimated at 13.0 $\mu g\ m^{-2}\ year^{-1}$ with 73% of the wet Hg deposition flux occurring in the rainy season. PHg constituted 53% of the THg deposition. The annual fluxes of THg throughfall deposition were 12.4 $\mu g\ m^{-2}$ for the south side of the forest watershed and 10.6 $\mu g\ m^{-2}$ for the north side. The throughfall DHg fluxes at the south side were significantly greater than the flux at the north side (7.8 $\mu g\ m^{-2}\ year^{-1}$ versus 5.8 $\mu g\ m^{-2}\ year^{-1}$).

The annual runoff was 384 mm, leading to 1.8 $\mu g\ m^{-2}\ year^{-1}$ THg flux (0.4 $\mu g\ m^{-2}\ year^{-1}$ DHg and 1.4 $\mu g\ m^{-2}\ year^{-1}$ PHg). Over 85% runoff Hg occurred in the rainy season. There was a rainstorm in June 2022, which sharply increased the runoff Hg flux and contributed to 1.2 $\mu g\ m^{-2}\ year^{-1}$ in the month.

3.3. Hg Isotopic Signatures. Figure 2 shows the isotopic compositions of Hg species in the dry and rainy seasons (Tables S1−S3). The Hg isotopic signatures in atmospheric Hg^0 were δ^{202}Hg = 1.19 ± 0.58‰, Δ^{199}Hg = −0.11 ± 0.05‰, Δ^{200}Hg = −0.04 ± 0.04‰, Δ^{201}Hg = −0.08 ± 0.06‰, and Δ^{204}Hg = 0.07 ± 0.12‰ ($n = 28$) without seasonal differences (Table S4). The DHg of open-field precipitation displayed slightly negative MDF and positive odd- and even-MIF signatures without any seasonal trend, with δ^{202}Hg = −0.34 ± 0.47‰, Δ^{199}Hg = 0.54 ± 0.25‰, Δ^{200}Hg = 0.20 ± 0.06‰, Δ^{201}Hg = 0.57 ± 0.26‰, and Δ^{204}Hg = −0.29 ± 0.16‰ ($n = 25$; Figure 2A−D and Table S2). The isotopic signatures in throughfall DHg pointed from signals of precipitation to litterfall (δ^{202}Hg = −2.31 ± 0.13‰, Δ^{199}Hg = −0.32 ± 0.05‰, and Δ^{200}Hg = −0.04 ± 0.03‰).[50] The isotopic signatures in throughfall samples were −1.77 ± 0.56‰ of δ^{202}Hg, 0.17 ± 0.24‰ of Δ^{199}Hg, 0.05 ± 0.07‰ of Δ^{200}Hg, 0.14 ± 0.22‰ of Δ^{201}Hg, and −0.07 ± 0.16‰ of Δ^{204}Hg ($n = 36$; Table S2). δ^{202}Hg was comparable in rainy and dry seasons, while Δ^{199}Hg was more negative (∼-0.18‰) in the rainy season than in the dry season. We observed more negative δ^{202}Hg and Δ^{199}Hg at the south side throughfall in contrast to those at the north side in the rainy season, while the difference was insignificant in the dry season. In addition, runoff DHg had the isotopic compositions of δ^{202}Hg = −1.19 ± 0.78‰, Δ^{199}Hg = −0.02 ± 0.04‰, Δ^{200}Hg = 0.04 ± 0.04‰, Δ^{201}Hg = −0.04 ± 0.03‰, and Δ^{204}Hg = −0.01 ± 0.15‰ ($n = 6$) in the dry season and δ^{202}Hg = −1.61 ± 0.18‰, Δ^{199}Hg = −0.10 ± 0.03‰, Δ^{200}Hg = −0.01 ± 0.04‰, Δ^{201}Hg = −0.12 ± 0.03‰, and Δ^{204}Hg = 0.01 ± 0.04‰ ($n = 4$) in the rainy season (Table S3).

Precipitation PHg displayed a δ^{202}Hg value of −0.59 ± 0.37‰, Δ^{199}Hg of 0.18 ± 0.11‰, Δ^{200}Hg of 0.17 ± 0.06‰, Δ^{201}Hg of 0.13 ± 0.07‰, and Δ^{204}Hg of −0.31 ± 0.20‰ ($n = 4$) in the dry season and δ^{202}Hg of −0.73 ± 0.48‰, Δ^{199}Hg of 0.37 ± 0.09‰, Δ^{200}Hg of 0.18 ± 0.01‰, Δ^{201}Hg of 0.47 ± 0.19‰, and Δ^{204}Hg of −0.38 ± 0.04‰ ($n = 4$) in the rainy season (Figure 2E−H). Throughfall PHg showed values of −1.58 ± 0.27‰ for δ^{202}Hg, −0.24 ± 0.13‰ for Δ^{199}Hg, 0.00 ± 0.04‰ for Δ^{200}Hg, −0.25 ± 0.13‰ for Δ^{201}Hg, and 0.00 ± 0.10‰ for Δ^{204}Hg ($n = 21$; Table S2). The seasonal and spatial trends were insignificant. The isotopic signatures in runoff PHg showed little seasonal trend, as δ^{202}Hg = −1.46 ± 0.11‰, Δ^{199}Hg = −0.30 ± 0.05‰, Δ^{200}Hg = −0.04 ± 0.04‰, Δ^{201}Hg = −0.30 ± 0.04‰, and Δ^{204}Hg = 0.05 ± 0.08‰ ($n = 10$; Table S3).

The two-endmember mixing model results are detailed in Table S5. The mean contributions of atmospheric Hg^0 to PHg of throughfall were 69 ± 14% for the rainy season and 77 ± 11% for the dry season, and those to DHg were 62 ± 18% for the rainy season and 58 ± 18% for the dry season. The contribution of atmospheric Hg^0 in throughfall at the south side averaged at 74 ± 11% without seasonal difference. The contribution of atmospheric Hg^0 in throughfall at the north side annually averaged at 60 ± 20%. Additionally, atmospheric Hg^0 accounted for 84 ± 10% in the rainy season and 59 ± 14% in the dry season for runoff DHg and 97 ± 1% in the rainy season and 81 ± 10% in the dry season for runoff PHg.

4. DISCUSSION

4.1. Hg Sources in Throughfall. The median value of 7.7 ng L^{-1} THg concentration in open-field precipitation is comparable to values in remote Amazonian tropical forests (median of 9.2−9.8 ng L^{-1})[23,60] and in a remote broadleaf forest of China (median of 6.3 ng L^{-1}).[12] The THg concentration in throughfall was comparable to observations in remote Amazonian tropical forests with a median of 16−20 ng L^{-1}.[12,24] The open-field rainfall Hg deposition (13.0 $\mu g\ m^{-2}\ year^{-1}$) flux is comparable to observations in background forests (9.3 ± 4.3 $\mu g\ m^{-2}\ year^{-1}$).[12] However, the throughfall flux in this tropical rainforest (11.5 ± 1.2 $\mu g\ m^{-2}\ year^{-1}$) is 1−2 times lower than the reported throughfall fluxes in Amazon tropical rainforests (20−34 $\mu g\ m^{-2}\ year^{-1}$) due to the higher throughfall amount in Amazon tropical rainforests.

We observed the distinct positive δ^{202}Hg, negative Δ^{199}Hg and Δ^{200}Hg signatures of atmospheric Hg^0, which is comparable to observations of background atmospheric Hg^0 in Southwest China (δ^{202}Hg = 0.36 ± 0.35‰, Δ^{199}Hg = −0.12 ± 0.09‰, and Δ^{200}Hg = −0.04 ± 0.04‰).[35,43,44,61]

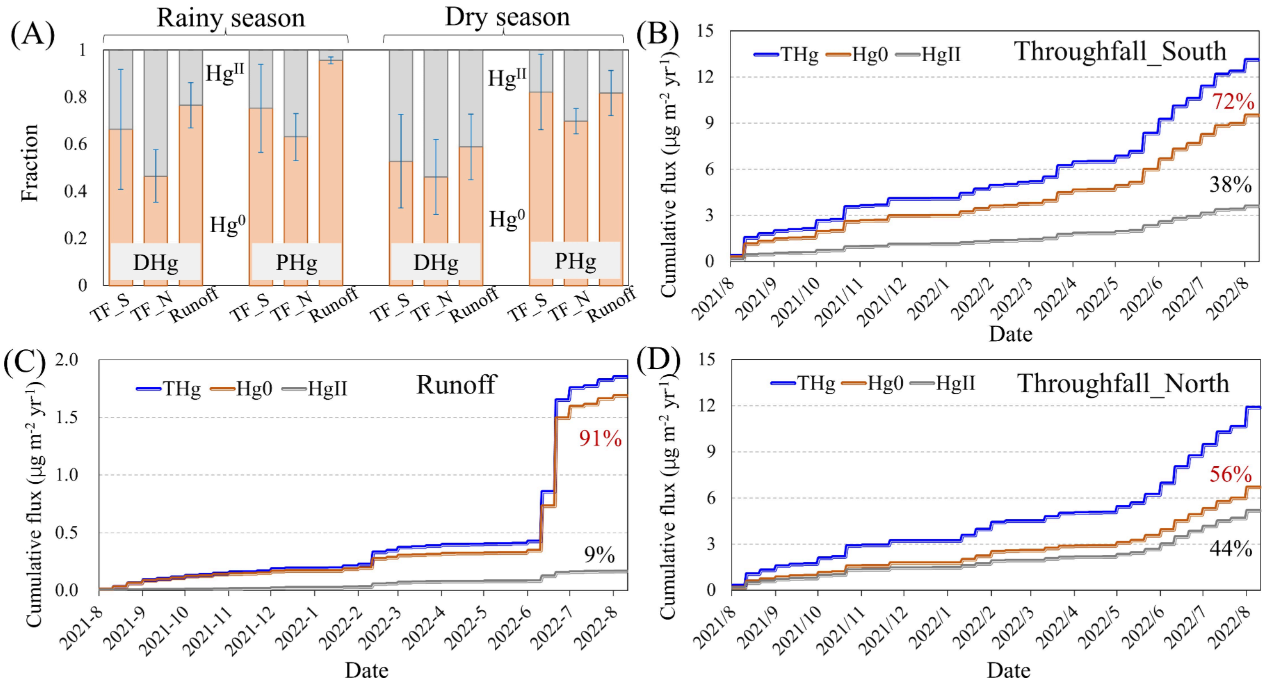

Figure 3. Source apportionment by the mercury (Hg) isotopic model and cumulative Hg flux in throughfall and runoff. (A) Source estimations for throughfall (south and north) and runoff. (B−D) Cumulative THg flux (in blue line), Hg^0 flux (in orange line), and Hg^{II} flux (in gray line) in throughfall on the south side and runoff and throughfall on the north side.

Additionally, we observed distinctive positive $\Delta^{199}Hg$ and $\Delta^{200}Hg$ signatures of open-field precipitation of DHg and PHg. Their values are around 0.20‰, consistent with the global atmospheric precipitation mean values of 0.23‰.[39−42,53,62] The PHg in precipitation shows a more negative $\Delta^{199}Hg$ value than DHg (0.28 ± 0.14‰ versus 0.54 ± 0.25‰). This is consistent with observations in North America and Tibetan Plateau.[39,40,63,64] The cloud droplet accumulation in atmospheric particle and rainfall water scavenging processes can incorporate the atmospheric particulate-bound Hg (PBM) into wet deposition.[39,40,63] This also can be supported by the isotopic evidence because of the comparable $\Delta^{199}Hg$ signatures between PHg in rainfall and PBM in air (0.40 ± 0.36‰ in remote regions).[65−67]

Throughfall Hg has more negative signals of MDF and MIF than open-field precipitation Hg (Figure 2). The Hg concentration in throughfall (13.5−16.2 ng L^{-1}) is 1.5−2 times higher compared to the values in open-field precipitation (190−260% higher for DHg and 150% higher for PHg, Figure 1). These observations suggest that the additional Hg sources with negative signals of MDF and MIF mixed into the rainfall when water passes through the canopy. The significantly negative correlations of DOC to $\delta^{202}Hg$ and $\Delta^{200}Hg$ in DHg ($p < 0.05$, Figure S3) further suggest the Hg source on the canopy with the elevated organic matter and negative signals of $\delta^{202}Hg$ and $\Delta^{200}Hg$. The additional Hg in throughfall can be mainly derived from Hg^{2+} and Hg^P already deposited on the canopy surface being washed into throughfall.[68,69] However, the isotopic signatures in throughfall do not support this process, because both atmospheric Hg^{2+} and Hg^P have the positive $\Delta^{199}Hg$ and $\Delta^{200}Hg$ signals,[65,67] which cannot induce the negative transition observed in the throughfall.

Figure 2 shows that the Hg isotopic compositions of throughfall DHg and PHg range between the signals of precipitation Hg^{2+} and atmospheric Hg^0. Hence, it is hypothesized that the additional Hg in throughfall (compared to open-field precipitation) is predominantly from atmospheric Hg^0 uptake by the canopy. The $\Delta^{200}Hg$ source mixing model confirmed this hypothesis. Averagely, the contribution of atmospheric Hg^0 in throughfall was 67 ± 12% in our tropical rainforest. Earlier studies suggest that the Hg^0 sources in the throughfall of coniferous forests are mainly from Hg^0 uptake by foliage, bark, moss, and lichen grown on the canopy and the subsequent detritus mixing into precipitation.[33] The taller canopy height and denser structure in the tropical rainforest further promote the atmospheric Hg^0 mixing into throughfall due to the fact that higher vegetation biomass induced the elevated Hg^0 uptake in tropical rainforests.[50,70] We observed the greater atmospheric Hg^0 contribution and DHg concentrations at the south side throughfall compared to the north side (Figures 2 and 3) because of a much more intensive canopy height at the south side. The greater atmospheric Hg^0 contribution in throughfall PHg than in DHg also confirms the process of Hg from canopy detritus dissolving in throughfall water.

Previous studies have estimated that the atmospheric Hg^0 source contributed to 54% of Hg in throughfall in a subtropical karst forest and 82% in a mature alpine coniferous forest.[33,62] The different source contributions can be attributed to two aspects. One is that the taller canopy height of the tropical forest and alpine coniferous forest increases the atmospheric Hg^0 contribution, while the lower canopy height (5−8 m) of the subtropical karst forest decreases the atmospheric Hg^0 contribution.[33,62] The other is that substantial epiphytes in the alpine coniferous forest canopy in contrast to the subtropical karst forest led to a higher contribution of atmospheric Hg^0.[33]

4.2. Hg Sources in the Runoff.

Runoff comes from excessive precipitation escaping from forest ecosystems.[22,31,36,71] We compare the Hg concentrations and fluxes of runoff, open-field rainfall, and throughfall. The runoff DHg

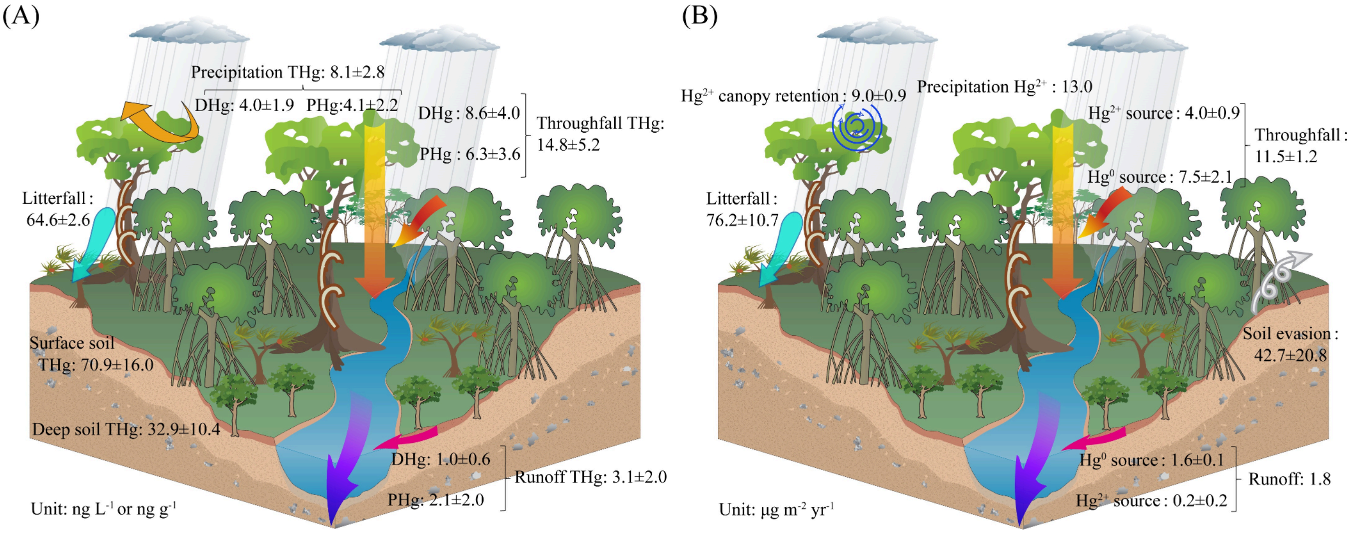

Figure 4. Summary of (A) Hg concentrations and (B) annual Hg fluxes of litterfall, rainfall, throughfall, and runoff for different Hg sources. The litterfall concentration and deposition flux are from Xia et al.[50] The soil evasion flux is investigated at a nearby tropical rainforest (~80 km far away from this study site), which is from Yuan et al.[61]

concentration is about 1/4 of the rainfall DHg and 1/8 of the throughfall DHg concentrations. The forest floor is rich in decomposing organics and could retain the Hg carried by throughfall and rainfall.[12] The comparable runoff DHg (1.0 ng L^{-1} vs 1.1 ng L^{-1}) and PHg concentration (2.0 ng L^{-1} vs 2.1 ng L^{-1}) between rainy and dry seasons further indicate Hg interception by the forest floor. The runoff THg flux is significantly lower than open-field precipitation and throughfall THg fluxes.

The δ^{202}Hg signatures of DHg in runoff water are among values of throughfall DHg, rainfall DHg, litter Hg, and surface soil Hg (Figure 2). Rainwater leaching processes lead to the dissolution and desorption of Hg from litter and soil into runoff water.[20−22] This suggests that, in addition to Hg from throughfall and rainfall, Hg desorption from decomposed litter and surface soil contributes to Hg in runoff. Heavier Hg isotopes tend to be enriched in the dissolved free Hg^{2+} during the Hg partitioning between the dissolved and particulate phases.[72,73] However, this is unlikely in the runoff processes because leaching Hg−DOM complexes does not lead to a distinct Hg-MDF shift.[36]

The slightly negative Δ^{199}Hg values in runoff DHg (−0.02 ± 0.05‰ in the dry season and −0.10 ± 0.03‰ in the rainy season) also suggest Hg contribution from rainfall and throughfall that shows relatively positive Δ^{199}Hg signals. PHg in runoff shows primarily negative Δ^{199}Hg (−0.28 ± 0.05‰ in the dry season and −0.34 ± 0.04‰ in the rainy season), similar to the Δ^{199}Hg values in PHg of throughfall (−0.24 ± 0.13‰), litterfall Hg (−0.32 ± 0.05‰), and surface soil Hg (−0.35 ± 0.05‰).[50] The forest floor can intercept rainfall and throughfall particulates during runoff, as evidenced by the depleted PHg concentration. Thus, PHg from decomposed biomasses and surface soil is the additional PHg source in the runoff.

We applied the Hg isotopic mixing model to quantify the Hg source contributions in runoff (Figure 3). The contribution of atmospheric Hg^0 for runoff is significantly higher in the rainy season than that in the dry season (84 ± 10% versus 59 ± 14% for DHg and 97 ± 1% versus 81 ± 10% for PHg) while without seasonal differences in throughfall. The greater runoff flow in the rainy season promotes the desorption of surface soil Hg into runoff water. The lower contribution of atmospheric Hg^0 in DHg than in PHg of runoff is because runoff DHg comes from multiple Hg sources (e.g., rainfall, throughfall, and forest soil desorption), while PHg is mainly from the organic soil particle and throughfall PHg.

4.3. Hg Flux Budget in Water. Combining the Hg isotopic model results, Hg concentrations, and fluxes (Figure 4A), the atmospheric Hg^0 and Hg^{2+} mass flows were estimated by eqs 7 and 8. We assumed that atmospheric Hg^{2+} dry deposition on the canopy surface is lower than precipitation Hg^{2+} deposition due to the high frequency of rainfall in this tropical region.[33] Given the large soil Hg reservoir,[46] the transient Hg input by hydrological processes does not distinctly influence soil Hg pool size. Based on these assumptions, we estimated the lower limit of atmospheric Hg^{2+} canopy retention flux and forest floor retention flux by eqs 7 and 8.

Figure 4B shows the flux of Hg sources in the whole ecosystem. The precipitation Hg^{2+} flux is 13.0 μg m^{-2} $year^{-1}$, of which 69 ± 7% of this Hg input is retained by the forest canopy. Therefore, 4.0 ± 0.9 μg m^{-2} $year^{-1}$ of atmospheric Hg^{2+} deposits onto the forest floor via throughfall. The atmospheric Hg^{2+} efflux via runoff water is 0.2 ± 0.2 μg m^{-2} $year^{-1}$, suggesting the forest floor Hg^{2+} retention flux of 3.8 ± 1.1 μg m^{-2} $year^{-1}$.

Up to 69% of atmospheric Hg^{2+} retention by the canopy is significantly higher than those reported in the alpine coniferous forest (37−48% retention flux).[33] The elevated canopy Hg^{2+} retention in this tropical rainforest is attributed to the taller canopy height and greater vegetation biomass compared to coniferous forests (height: 65 m vs 20−30 m; biomass: 769 g m^{-2} $year^{-1}$ vs 444 g m^{-2} $year^{-1}$).[33,50] The retained Hg^{2+} could re-emit back to the atmosphere after photoreduction[74] and be assimilated by epiphytes or sorbed by the canopy.[34,75]

The atmospheric Hg^0 deposition via litterfall is 76.2 ± 10.7 μg m^{-2} $year^{-1}$ (Figure 4B), about 20 times the atmospheric Hg^{2+} retention by the forest floor. This is consistent with earlier Hg isotopic evidence that up to 90% surface soil Hg is derived from atmospheric Hg^0 deposition.[76] In addition to adsorption by soil organic matter,[36,76] the retained atmospheric Hg^{2+} on the forest floor can be released back to the atmosphere after photochemical and microbial reduction.[45,75,77]

The atmospheric Hg^0 deposition via throughfall is 7.5 ± 2.1 $\mu g\ m^{-2}\ year^{-1}$, with its efflux via runoff at 1.6 ± 1.2 $\mu g\ m^{-2}\ year^{-1}$. Our earlier study in a nearby tropical rainforest (~80 km far away from this study site) showed 42.7 ± 20.8 $\mu g\ m^{-2}\ year^{-1}$ soil Hg evasion flux.[50,61] This suggests that the soil Hg^0 emission can significantly offset atmospheric Hg^0 inputs (nearly 83 $\mu g\ m^{-2}\ year^{-1}$). Such a small fraction of atmospheric Hg deposition can be finally stored in the soil, thus leading to the relatively low soil Hg concentration (70.9 ± 16.0 $ng\ g^{-1}$) in the tropical rainforest, which is only 1/3 to 1/2 of soil Hg concentrations in subtropical and boreal forests.[45,78,79]

5. IMPLICATIONS

Globally, the precipitation deposition ranges between 690 and 1000 Mg $year^{-1}$ and the throughfall Hg deposition ranges between 1100 and 1400 Mg $year^{-1}$.[5,10,12] Earlier studies attributed such elevated Hg flux in throughfall to the atmospheric Hg^{2+} dry deposition.[12] However, the findings of this study show that throughfall Hg is derived primarily from atmospheric Hg^0 deposition (by 67% on average). Combining 54% of Hg in throughfall in a subtropical karst forest,[62] 82% in a mature alpine coniferous forest,[33] and 67% in this study, we approximated the atmospheric Hg^0 deposition via throughfall to be in the range of 600−1000 Mg $year^{-1}$ globally, representing 60−80% of the atmospheric Hg^0 deposition via litterfall.[5,70] This suggests that treating throughfall Hg as atmospheric Hg^{2+} deposition would significantly underestimate the contribution of atmospheric Hg^0 to forest ecosystems. In the studied forest, 69% of atmospheric Hg^{2+} deposition is intercepted by tropical vegetation biomass. The newly deposited atmospheric Hg^{2+} on the surface of canopy vegetation can be reduced into Hg^0 and then re-emit back into air, offsetting the deposition flux of atmospheric Hg^0 uptake by foliage on the canopy. Finally, the small flux of runoff Hg suggests that Hg in rainfall and throughfall is largely retained by the canopy and rainforest floor, thus reducing the potential ecological risk to the downstream aquatic ecosystems.

■ ASSOCIATED CONTENT

Supporting Information

The Supporting Information is available free of charge at https://pubs.acs.org/doi/10.1021/acs.est.3c09265.

Additional experimental data sets in Sections S1 and S2 and Tables S1−S5 and additional figures as mentioned in the text in Figures S1−S3 (PDF)

Hg model input data (XLSX)

■ AUTHOR INFORMATION

Corresponding Authors

Xun Wang − *State Key Laboratory of Environmental Geochemistry, Institute of Geochemistry, Chinese Academy of Sciences, Guiyang 550081, China;* orcid.org/0000-0002-7407-8965; Email: wangxun@mail.gyig.ac.cn

Xinbin Feng − *State Key Laboratory of Environmental Geochemistry, Institute of Geochemistry, Chinese Academy of Sciences, Guiyang 550081, China; University of Chinese Academy of Sciences, Beijing 100049, China;* orcid.org/0000-0002-7462-8998; Email: fengxinbin@vip.skleg.cn

Authors

Wei Yuan − *State Key Laboratory of Environmental Geochemistry, Institute of Geochemistry, Chinese Academy of Sciences, Guiyang 550081, China*

Che-Jen Lin − *Center for Advances in Water and Air Quality, Lamar University, Beaumont, Texas 77710, United States*

Ge Zhang − *State Key Laboratory of Environmental Geochemistry, Institute of Geochemistry, Chinese Academy of Sciences, Guiyang 550081, China; College of Resource and Environmental Engineering, Guizhou University, Guiyang 550025, China*

Fei Wu − *State Key Laboratory of Environmental Geochemistry, Institute of Geochemistry, Chinese Academy of Sciences, Guiyang 550081, China; University of Chinese Academy of Sciences, Beijing 100049, China*

Nantao Liu − *State Key Laboratory of Environmental Geochemistry, Institute of Geochemistry, Chinese Academy of Sciences, Guiyang 550081, China;* orcid.org/0009-0003-5151-9849

Longyu Jia − *State Key Laboratory of Environmental Geochemistry, Institute of Geochemistry, Chinese Academy of Sciences, Guiyang 550081, China; University of Chinese Academy of Sciences, Beijing 100049, China*

Hui Zhang − *State Key Laboratory of Environmental Geochemistry, Institute of Geochemistry, Chinese Academy of Sciences, Guiyang 550081, China*

Huazheng Lu − *CAS Key Laboratory of Tropical Forest Ecology, Xishuangbanna Tropical Botanical Garden, Chinese Academy of Sciences, Mengla 666303, China*

Jinlong Dong − *CAS Key Laboratory of Tropical Forest Ecology, Xishuangbanna Tropical Botanical Garden, Chinese Academy of Sciences, Mengla 666303, China; University of Chinese Academy of Sciences, Beijing 100049, China*

Complete contact information is available at:
https://pubs.acs.org/10.1021/acs.est.3c09265

Notes

The authors declare no competing financial interest.

■ ACKNOWLEDGMENTS

This work was funded by the National Natural Science Foundation of China (42377255, 42394093, and 42007307) and Youth Innovation Promotion Association CAS (grants 2023418 and 2022404). We appreciate the Xishuangbanna Station for Tropical Rain Forest Ecosystem Studies (XSTRE) for providing climate information and assistance in the field study. We also thank Dr. Luxiang Lin, Dr. Yun Deng, and Mr. Jinhai Mu for sampling in the field. The data used in this study are tabulated in the Supporting Information.

■ REFERENCES

(1) Pirrone, N.; Hedgecock, I. M.; Sprovieri, F. New Directions: Atmospheric mercury, easy to spot and hard to pin down: impasse? *Atmos. Environ.* **2008**, *42* (36), 8549−8551.

(2) Streets, D. G.; Horowitz, H. M.; Jacob, D. J.; Lu, Z.; Levin, L.; Ter Schure, A. F. H.; Sunderland, E. M. Total Mercury Released to the Environment by Human Activities. *Environ. Sci. Technol.* **2017**, *51* (11), 5969−5977.

(3) Schroeder, W. H.; Munthe, J. Atmospheric mercury - An overview. *Atmos. Environ.* **1998**, *32* (5), 809−822.

(4) Obrist, D.; Roy, E. M.; Harrison, J. L.; Kwong, C. F.; Munger, J. W.; Moosmuller, H.; Romero, C. D.; Sun, S.; Zhou, J.; Commane, R. Previously unaccounted atmospheric mercury deposition in a midlatitude deciduous forest. *Proc. Natl. Acad. Sci. U. S. A.* **2021**, *118* (29), e2105477118.

(5) Zhou, J.; Obrist, D. Global Mercury Assimilation by Vegetation. *Environ. Sci. Technol.* **2021**, *55* (20), 14245−14257.

(6) Wang, X.; Yuan, W.; Lin, C. J.; Wu, F.; Feng, X. Stable mercury isotopes stored in Masson Pinus tree rings as atmospheric mercury archives. *J. Hazard Mater.* **2021**, *415*, No. 125678.

(7) Selin, H.; Keane, S. E.; Wang, S.; Selin, N. E.; Davis, K.; Bally, D. Linking science and policy to support the implementation of the Minamata Convention on Mercury. *Ambio* **2018**, *47* (2), 198−215.

(8) Selin, N. E. Global Biogeochemical Cycling of Mercury: A Review. *Annu. Rev. Env Resour* **2009**, *34*, 43−63.

(9) Wang, X.; Luo, J.; Yuan, W.; Lin, C. J.; Wang, F.; Liu, C.; Wang, G.; Feng, X. Global warming accelerates uptake of atmospheric mercury in regions experiencing glacier retreat. *Proc. Natl. Acad. Sci. U. S. A.* **2020**, *117* (4), 2049−2055.

(10) Fu, X.; Zhu, W.; Zhang, H.; Sommar, J.; Yu, B.; Yang, X.; Wang, X.; Lin, C. J.; Feng, X. Depletion of atmospheric gaseous elemental mercury by plant uptake at Mt. Changbai, Northeast China. *Atmos. Chem. Phys.* **2016**, *16* (20), 12861−12873.

(11) Agnan, Y.; Le Dantec, T.; Moore, C. W.; Edwards, G. C.; Obrist, D. New Constraints on Terrestrial Surface Atmosphere Fluxes of Gaseous Elemental Mercury Using a Global Database. *Environ. Sci. Technol.* **2016**, *50* (2), 507−524.

(12) Wang, X.; Yuan, W.; Lin, C. J.; Feng, X. B. Mercury cycling and isotopic fractionation in global forests. *Critical Reviews in Environmental Science and Technology* **2022**, *52* (21), 3763−3786.

(13) FAO, *The State of the World's Forests 2020*. 2021.

(14) Hölscher, D.; Sá, T. D. A.; Möller, R. F.; Denich, M.; Fölster, H. Rainfall partitioning and related hydrochemical fluxes in a diverse and in a mono specific (Phenakospermum guyannense) secondary vegetation stand in eastern Amazonia. *Oecologia* **1998**, *114* (2), 251−257.

(15) Siles, P.; Vaast, P.; Dreyer, E.; Harmand, J.-M. Rainfall partitioning into throughfall, stemflow and interception loss in a coffee (Coffea arabica L.) monoculture compared to an agroforestry system with Inga densiflora. *Journal of Hydrology* **2010**, *395* (1), 39−48.

(16) Park, A.; Cameron, J. L. The influence of canopy traits on throughfall and stemflow in five tropical trees growing in a Panamanian plantation. *Forest Ecol Manag* **2008**, *255* (5), 1915−1925.

(17) Dietz, J.; Hölscher, D.; Leuschner, C.; Hendrayanto. Hendrayanto, Rainfall partitioning in relation to forest structure in differently managed montane forest stands in Central Sulawesi, Indonesia. *For. Ecol. Manage.* **2006**, *237* (1-3), 170−178.

(18) Potapov, P.; Li, X.; Hernandez-Serna, A.; Tyukavina, A.; Hansen, M. C.; Kommareddy, A.; Pickens, A.; Turubanova, S.; Tang, H.; Silva, C. E.; Armston, J.; Dubayah, R.; Blair, J. B.; Hofton, M. Mapping global forest canopy height through integration of GEDI and Landsat data. *Remote Sensing of Environment* **2021**, *253*, No. 112165.

(19) Cao, M.; Zou, X.; Warren, M.; Zhu, H. Tropical Forests of Xishuangbanna, China1. *Biotropica* **2006**, *38* (3), 306−309.

(20) Zhao, Z.; Wang, D.; Wang, Y.; Mu, Z.; Zhu, J. Wet deposition flux and runoff output flux of mercury in a typical small agricultural watershed in Three Gorges Reservoir areas. *Environmental Science and Pollution Research* **2015**, *22* (7), 5538−5551.

(21) Schwesig, D.; Matzner, E. Dynamics of mercury and methylmercury in forest floor and runoff of a forested watershed in Central Europe. *Biogeochemistry* **2001**, *53* (2), 181−200.

(22) Allan, C. J.; Heyes, A.; Roulet, N. T.; St. Louis, V. L.; Rudd, J. W. M. Spatial and temporal dynamics of mercury in Precambrian Shield upland runoff. *Biogeochemistry* **2001**, *52* (1), 13−40.

(23) Fostier, A. H.; Forti, M. C.; Guimaraes, J. R. D.; Melfi, A. J.; Boulet, R.; Santo, C. M. E.; Krug, F. J. Mercury fluxes in a natural forested Amazonian catchment (Serra do Navio, Amapa State, Brazil). *Sci. Total Environ.* **2000**, *260* (1−3), 201−211.

(24) Gerson, J. R.; Szponar, N.; Zambrano, A. A.; Bergquist, B.; Broadbent, E.; Driscoll, C. T.; Erkenswick, G.; Evers, D. C.; Fernandez, L. E.; Hsu-Kim, H.; Inga, G.; Lansdale, K. N.; Marchese, M. J.; Martinez, A.; Moore, C.; Pan, W. K.; Purizaca, R. P.; Sánchez, V.; Silman, M.; Ury, E. A.; Vega, C.; Watsa, M.; Bernhardt, E. S. Amazon forests capture high levels of atmospheric mercury pollution from artisanal gold mining. *Nat. Commun.* **2022**, *13* (1), 559.

(25) St Louis, V. L.; Graydon, J. A.; Lehnherr, I.; Amos, H. M.; Sunderland, E. M.; St Pierre, K. A.; Emmerton, C. A.; Sandilands, K.; Tate, M.; Steffen, A.; Humphreys, E. R. Atmospheric Concentrations and Wet/Dry Loadings of Mercury at the Remote Experimental Lakes Area, Northwestern Ontario, Canada. *Environ. Sci. Technol.* **2019**, *53* (14), 8017−8026.

(26) Wright, L. P.; Zhang, L. M.; Marsik, F. J. Overview of mercury dry deposition, litterfall, and throughfall studies. *Atmos Chem. Phys.* **2016**, *16* (21), 13399−13416.

(27) Moreno-Brush, M.; McLagan, D. S.; Biester, H. Fate of mercury from artisanal and small-scale gold mining in tropical rivers: Hydrological and biogeochemical controls. A critical review. *Critical Reviews in Environmental Science and Technology* **2020**, *50* (5), 437−475.

(28) Lindberg, S.; Bullock, R.; Ebinghaus, R.; Engstrom, D.; Feng, X.; Fitzgerald, W.; Pirrone, N.; Prestbo, E.; Seigneur, C.; Panel on Source Attribution of Atmospheric, M., A synthesis of progress and uncertainties in attributing the sources of mercury in deposition. *Ambio* **2007**, *36*, (1), 19−32.

(29) Yu, Q.; Luo, Y.; Xu, G.; Wu, Q.; Wang, S.; Hao, J.; Duan, L. Subtropical Forests Act as Mercury Sinks but as Net Sources of Gaseous Elemental Mercury in South China. *Environ. Sci. Technol.* **2020**, *54* (5), 2772−2779.

(30) Zhou, J.; Feng, X. B.; Liu, H. Y.; Zhang, H.; Fu, X. W.; Bao, Z. D.; Wang, X.; Zhang, Y. P. Examination of total mercury inputs by precipitation and litterfall in a remote upland forest of Southwestern China. *Atmos. Environ.* **2013**, *81*, 364−372.

(31) Bishop, K.; Shanley, J. B.; Riscassi, A.; de Wit, H. A.; Eklof, K.; Meng, B.; Mitchell, C.; Osterwalder, S.; Schuster, P. F.; Webster, J.; Zhu, W. Recent advances in understanding and measurement of mercury in the environment: Terrestrial Hg cycling. *Sci. Total Environ.* **2020**, *721*, No. 137647.

(32) Sommar, J.; Osterwalder, S.; Zhu, W. Recent advances in understanding and measurement of Hg in the environment: Surface-atmosphere exchange of gaseous elemental mercury (Hg(0)). *Sci. Total Environ.* **2020**, *721*, No. 137648.

(33) Wang, X.; Yuan, W.; Lin, C. J.; Luo, J.; Wang, F.; Feng, X.; Fu, X.; Liu, C. Underestimated Sink of Atmospheric Mercury in a Deglaciated Forest Chronosequence. *Environ. Sci. Technol.* **2020**, *54* (13), 8083−8093.

(34) Li, X.; Wang, X.; Zhang, H.; Lu, Z. Mosses and lichens enhance atmospheric elemental mercury deposition in a subtropical montane forest. *Environmental Chemistry* **2023**, *20* (3), 105−113.

(35) Yuan, W.; Sommar, J.; Lin, C. J.; Wang, X.; Li, K.; Liu, Y.; Zhang, H.; Lu, Z.; Wu, C.; Feng, X. Stable Isotope Evidence Shows Re-emission of Elemental Mercury Vapor Occurring after Reductive Loss from Foliage. *Environ. Sci. Technol.* **2019**, *53* (2), 651−660.

(36) Jiskra, M.; Wiederhold, J. G.; Skyllberg, U.; Kronberg, R. M.; Kretzschmar, R. Source tracing of natural organic matter bound mercury in boreal forest runoff with mercury stable isotopes. *Environ. Sci. Process Impacts* **2017**, *19* (10), 1235−1248.

(37) Woerndle, G. E.; Tsz-Ki Tsui, M.; Sebestyen, S. D.; Blum, J. D.; Nie, X.; Kolka, R. K. New Insights on Ecosystem Mercury Cycling Revealed by Stable Isotopes of Mercury in Water Flowing from a Headwater Peatland Catchment. *Environ. Sci. Technol.* **2018**, *52* (4), 1854−1861.

(38) Sonke, J. E.; Angot, H.; Zhang, Y.; Poulain, A.; Björn, E.; Schartup, A. Global change effects on biogeochemical mercury cycling. *Ambio* **2023**, *52* (5), 853−876.

(39) Yuan, S.; Chen, J.; Hintelmann, H.; Cai, H.; Yuan, W.; He, S.; Zhang, K.; Zhang, Y.; Liu, Y. Event-Based Atmospheric Precipitation Uncovers Significant Even and Odd Hg Isotope Anomalies Associated with the Circumpolar Vortex. *Environ. Sci. Technol.* **2022**, *56* (17), 12713−12722.

(40) Chen, J. B.; Hintelmann, H.; Feng, X. B.; Dimock, B. Unusual fractionation of both odd and even mercury isotopes in precipitation from Peterborough, ON, Canada. *Geochim. Cosmochim. Acta* **2012**, *90*, 33−46.

(41) Demers, J. D.; Blum, J. D.; Zak, D. R. Mercury isotopes in a forested ecosystem: Implications for air-surface exchange dynamics and the global mercury cycle. *Global Biogeochem Cy* **2013**, *27* (1), 222−238.

(42) Gratz, L. E.; Keeler, G. J.; Blum, J. D.; Sherman, L. S. Isotopic composition and fractionation of mercury in Great Lakes precipitation and ambient air. *Environ. Sci. Technol.* **2010**, *44* (20), 7764−70.

(43) Yu, B.; Fu, X.; Yin, R.; Zhang, H.; Wang, X.; Lin, C. J.; Wu, C.; Zhang, Y.; He, N.; Fu, P.; Wang, Z.; Shang, L.; Sommar, J.; Sonke, J. E.; Maurice, L.; Guinot, B.; Feng, X. Isotopic Composition of Atmospheric Mercury in China: New Evidence for Sources and Transformation Processes in Air and in Vegetation. *Environ. Sci. Technol.* **2016**, *50* (17), 9262−9.

(44) Fu, X.; Zhang, H.; Liu, C.; Zhang, H.; Lin, C. J.; Feng, X. Significant Seasonal Variations in Isotopic Composition of Atmospheric Total Gaseous Mercury at Forest Sites in China Caused by Vegetation and Mercury Sources. *Environ. Sci. Technol.* **2019**, *53* (23), 13748−13756.

(45) Yuan, W.; Wang, X.; Lin, C. J.; Wu, C.; Zhang, L.; Wang, B.; Sommar, J.; Lu, Z.; Feng, X. Stable Mercury Isotope Transition during Postdepositional Decomposition of Biomass in a Forest Ecosystem over Five Centuries. *Environ. Sci. Technol.* **2020**, *54* (14), 8739−8749.

(46) Wang, X.; Yuan, W.; Lin, C. J.; Zhang, L.; Zhang, H.; Feng, X. Climate and Vegetation As Primary Drivers for Global Mercury Storage in Surface Soil. *Environ. Sci. Technol.* **2019**, *53* (18), 10665−10675.

(47) Wang, X.; Yuan, W.; Lu, Z. Y.; Lin, C. J.; Yin, R. S.; Li, F.; Feng, X. B. Effects of Precipitation on Mercury Accumulation on Subtropical Montane Forest Floor: Implications on Climate Forcing. *J. Geophys Res-Biogeo* **2019**, *124* (4), 959−972.

(48) Blum, J. D.; Sherman, L. S.; Johnson, M. W. Mercury Isotopes in Earth and Environmental Sciences. *Annu. Rev. Earth Pl Sc* **2014**, *42*, 249−269.

(49) Blum, J. D.; Johnson, M. W. Recent Developments in Mercury Stable Isotope Analysis. *Rev. Mineral Geochem* **2017**, *82*, 733−757.

(50) Xia, S.; Yuan, W.; Lin, L.; Yang, X.; Feng, X.; Li, X.; Liu, X.; Chen, P.; Zeng, S.; Wang, D.; Su, Q.; Wang, X. Latitudinal gradient for mercury accumulation and isotopic evidence for post-depositional processes among three tropical forests in Southwest China. *J. Hazard Mater.* **2022**, *429*, No. 128295.

(51) Fei, X.; Song, Q.; Zhang, Y.; Liu, Y.; Sha, L.; Yu, G.; Zhang, L.; Duan, C.; Deng, Y.; Wu, C.; Lu, Z.; Luo, K.; Chen, A.; Xu, K.; Liu, W.; Huang, H.; Jin, Y.; Zhou, R.; Li, J.; Lin, Y.; Zhou, L.; Fu, Y.; Bai, X.; Tang, X.; Gao, J.; Zhou, W.; Grace, J. Carbon exchanges and their responses to temperature and precipitation in forest ecosystems in Yunnan, Southwest China. *Sci. Total Environ.* **2018**, *616−617*, 824−840.

(52) Shen, T.; Corlett, R. T.; Collart, F.; Kasprzyk, T.; Guo, X.-L.; Patiño, J.; Su, Y.; Hardy, O. J.; Ma, W.-Z.; Wang, J.; Wei, Y.-M.; Mouton, L.; Li, Y.; Song, L.; Vanderpoorten, A. Microclimatic variation in tropical canopies: A glimpse into the processes of community assembly in epiphytic bryophyte communities. *J. Ecol.* **2022**, *110* (12), 3023−3038, DOI: 10.1111/1365-2745.14011.

(53) Li, K.; Lin, C. J.; Yuan, W.; Sun, G. Y.; Fu, X. W.; Feng, X. B. An improved method for recovering and preconcentrating mercury in natural water samples for stable isotope analysis. *J. Anal Atom Spectrom* **2019**, *34* (11), 2303−2313.

(54) US EPA *Method 1631: Revision E: Mercury in water by oxidation, purge and trap, and cold vapor atomic fluorescence spectrometry*; 2002.

(55) Sun, R. Y.; Enrico, M.; Heimburger, L. E.; Scott, C.; Sonke, J. E. A double-stage tube furnace-acid-trapping protocol for the preconcentration of mercury from solid samples for isotopic analysis. *Anal Bioanal Chem.* **2013**, *405* (21), 6771−6781.

(56) Fu, X. W.; Heimburger, L. E.; Sonke, J. E. Collection of atmospheric gaseous mercury for stable isotope analysis using iodine- and chlorine-impregnated activated carbon traps. *J. Anal Atom Spectrom* **2014**, *29* (5), 841−852.

(57) Bergquist, B. A.; Blum, J. D. Mass-dependent and -independent fractionation of hg isotopes by photoreduction in aquatic systems. *Science* **2007**, *318* (5849), 417−20.

(58) Estrade, N.; Carignan, J.; Sonke, J. E.; Donard, O. F. X. Measuring Hg Isotopes in Bio-Geo-Environmental Reference Materials. *Geostand Geoanal Res.* **2010**, *34* (1), 79−93.

(59) Wu, F.; Yang, L.; Wang, X.; Yuan, W.; Lin, C.-J.; Feng, X. Mercury Accumulation and Sequestration in a Deglaciated Forest Chronosequence: Insights from Particulate and Mineral-Associated Forms of Organic Matter. *Environ. Sci. Technol.* **2023**, *57* (43), 16512−16521.

(60) Fadini, P. S.; Jardim, W. F. Is the Negro River Basin (Amazon) impacted by naturally occurring mercury? *Sci. Total Environ.* **2001**, *275* (1−3), 71−82.

(61) Yuan, W.; Wang, X.; Lin, C.-J.; Song, Q.; Zhang, H.; Wu, F.; Liu, N.; Lu, H.; Feng, X. Deposition and Re-Emission of Atmospheric Elemental Mercury over the Tropical Forest Floor. *Environ. Sci. Technol.* **2023**, *57* (29), 10686−10695.

(62) Xia, J.; Wang, J.; Zhang, L.; Wang, X.; Yuan, W.; Peng, T.; Zheng, L.; Tian, W.; Feng, X. Migration and transformation of soil mercury in a karst region of southwest China: Implications for groundwater contamination. *Water Res.* **2022**, *226*, No. 119271.

(63) Yuan, S.; Chen, J.; Cai, H.; Yuan, W.; Wang, Z.; Huang, Q.; Liu, Y.; Wu, X. Sequential samples reveal significant variation of mercury isotope ratios during single rainfall events. *Sci. Total Environ.* **2018**, *624*, 133−144.

(64) Lepak, R. F.; Yin, R. S.; Krabbenhoft, D. P.; Ogorek, J. M.; DeWild, J. F.; Holsen, T. M.; Hurley, J. P. Use of Stable Isotope Signatures to Determine Mercury Sources in the Great Lakes. *Environ. Sci. Tech Let* **2015**, *2* (12), 335−341.

(65) Fu, X.; Zhang, H.; Feng, X.; Tan, Q.; Ming, L.; Liu, C.; Zhang, L. Domestic and Transboundary Sources of Atmospheric Particulate Bound Mercury in Remote Areas of China: Evidence from Mercury Isotopes. *Environ. Sci. Technol.* **2019**, *53* (4), 1947−1957.

(66) Huang, Q.; Chen, J.; Huang, W.; Fu, P.; Guinot, B.; Feng, X.; Shang, L.; Wang, Z.; Wang, Z.; Yuan, S.; Cai, H.; Wei, L.; Yu, B. Isotopic composition for source identification of mercury in atmospheric fine particles. *Atmos. Chem. Phys.* **2016**, *16* (18), 11773−11786.

(67) Liu, C.; Fu, X.; Xu, Y.; Zhang, H.; Wu, X.; Sommar, J.; Zhang, L.; Wang, X.; Feng, X. Sources and Transformation Mechanisms of Atmospheric Particulate Bound Mercury Revealed by Mercury Stable Isotopes. *Environ. Sci. Technol.* **2022**, *56* (8), 5224−5233.

(68) Rea, A. W.; Lindberg, S. E.; Keeler, G. J. Dry deposition and foliar leaching of mercury and selected trace elements in deciduous forest throughfall. *Atmos. Environ.* **2001**, *35* (20), 3453−3462, DOI: 10.1016/S1352-2310(01)00133-9.

(69) Zheng, W.; Obrist, D.; Weis, D.; Bergquist, B. A. Mercury isotope compositions across North American forests. *Global Biogeochem Cy* **2016**, *30* (10), 1475−1492.

(70) Wang, X.; Bao, Z.; Lin, C. J.; Yuan, W.; Feng, X. Assessment of Global Mercury Deposition through Litterfall. *Environ. Sci. Technol.* **2016**, *50* (16), 8548−57.

(71) Eklöf, K.; Meili, M.; Åkerblom, S.; von Brömssen, C.; Bishop, K. Impact of stump harvest on run-off concentrations of total mercury and methylmercury. *Forest Ecol Manag* **2013**, *290*, 83−94.

(72) Jiskra, M.; Wiederhold, J. G.; Bourdon, B.; Kretzschmar, R. Solution speciation controls mercury isotope fractionation of Hg(II) sorption to goethite. *Environ. Sci. Technol.* **2012**, *46* (12), 6654−62.

(73) Wiederhold, J. G.; Cramer, C. J.; Daniel, K.; Infante, I.; Bourdon, B.; Kretzschmar, R. Equilibrium mercury isotope fractiona-

tion between dissolved Hg(II) species and thiol-bound Hg. *Environ. Sci. Technol.* **2010**, *44* (11), 4191−7.

(74) Luo, Y.; Duan, L.; Driscoll, C. T.; Xu, G. Y.; Shao, M. S.; Taylor, M.; Wang, S. X.; Hao, J. M. Foliage/atmosphere exchange of mercury in a subtropical coniferous forest in south China. *J. Geophys Res-Biogeo* **2016**, *121* (7), 2006−2016.

(75) Tsui, M. T.-K.; Uzun, H.; Ruecker, A.; Majidzadeh, H.; Ulus, Y.; Zhang, H.; Bao, S.; Blum, J. D.; Karanfil, T.; Chow, A. T. Concentration and isotopic composition of mercury in a blackwater river affected by extreme flooding events. *Limnol. Oceanogr.* **2020**, *65* (9), 2158−2169, DOI: 10.1002/lno.11445.

(76) Jiskra, M.; Wiederhold, J. G.; Skyllberg, U.; Kronberg, R. M.; Hajdas, I.; Kretzschmar, R. Mercury deposition and re-emission pathways in boreal forest soils investigated with Hg isotope signatures. *Environ. Sci. Technol.* **2015**, *49* (12), 7188−96.

(77) Motta, L. C.; Blum, J. D.; Popp, B. N.; Umhau, B. P.; Benitez-Nelson, C. R.; Close, H. G.; Washburn, S. J.; Drazen, J. C. Mercury isotopic evidence for the importance of particles as a source of mercury to marine organisms. *Proc. Natl. Acad. Sci.* **2022**, *119* (44), No. e2208183119.

(78) Yuan, W.; Wang, X.; Lin, C.-J.; Zhang, H.; Feng, X.; Lu, Z. Impacts of Extreme Weather on Mercury Uptake and Storage in Subtropical Forest Ecosystems. *J. Geophys. Res.: Biogeosci.* **2022**, *127* (1), No. e2021JG006681.

(79) Obrist, D.; Johnson, D. W.; Lindberg, S. E.; Luo, Y.; Hararuk, O.; Bracho, R.; Battles, J. J.; Dail, D. B.; Edmonds, R. L.; Monson, R. K.; Ollinger, S. V.; Pallardy, S. G.; Pregitzer, K. S.; Todd, D. E. Mercury Distribution Across 14 US Forests. Part I: Spatial Patterns of Concentrations in Biomass, Litter, and Soils. *Environ. Sci. Technol.* **2011**, *45* (9), 3974−3981.